NASA DEVELOP National Program
Idaho – Pocatello
Summer 2021

Assateague Island National Seashore Ecological Forecasting

Characterizing Nearshore Suspended Sediments and Landcover Change Relative to Sediment Bypassing and Catastrophic Events

DEVELOP Technical Report
Final – August 12th, 2021

M. Colin Marvin (Project Lead)
Porter Abbey
Jay Mrazek
Erin Weitzel
Remi Work

Advisor:
Keith Weber (Idaho State University, GIS Training and Research Center)

1. Abstract

Assateague Island is located off the coast of Maryland and Virginia and serves as a home to sensitive species and habitats. However, infrastructure development disrupted the natural sediment transport processes of the barrier island, which accelerated erosion of the island's shoreline. To counteract this, the United States Army Corps of Engineers (USACE) initiated semiannual sediment bypassing operations in 2004. Over time, financial constraints limited the amount of sediment deposition possible, leading to concerns over navigational issues in nearby channels and the possibility of the operations not providing their intended benefits. To address these issues, NASA DEVELOP partnered with the National Park Service and USACE. The team performed time series analyses of nearshore suspended sediment from 2004-2020 and landcover change from 2006-2018 with satellite imagery from Landsat 5 Thematic Mapper (TM), Landsat 7 Enhanced Thematic Mapper Plus (ETM+), Landsat 8 Operational Land Imager (OLI), and Sentinel-2 MultiSpectral Instrument (MSI). The sediment transport analyses showed that suspended sediment levels are seasonally dependent. Meanwhile, historical land cover trends included a net increase in unconsolidated shore and a net decrease in open water. Land cover change was then forecast to 2021, 2031, and 2046 using the IDRISI TerrSet Land Change Modeler. The model predicted the most drastic land cover changes in the southern portion and the least on the eastern foreshore of the island. As a result, this project allows our partners to understand the impact of sediment bypassing operations more fully and make better-informed decisions regarding the island's management.

Key Terms
remote sensing, sediment bypassing, land cover change, Random Forest, IDRISI TerrSet, piping plover, ocean color

2. Introduction

2.1 Background Information

In 1933, a massive hurricane swept across New England and created the Ocean City inlet, forming Assateague Island to the south and Fenwick Island to the north by segmenting the preexisting barrier island (Schupp, 2013). To stabilize the land, the United States Army Corps of Engineers (USACE) constructed the Ocean City inlet jetty system in 1935, thereby interrupting the natural sediment transport to Assateague Island, leading to accelerated erosion of the shoreline (National Park Service, 2017). To mitigate this, USACE initiated the North End Restoration project. In 2002, a short-term beach nourishment effort was performed, and in 2004, long-term sediment bypassing operations commenced with semi-annual dredging of sediment from the inlet area and subsequent deposition on the island's nearshore (Zimmerman, 2004).

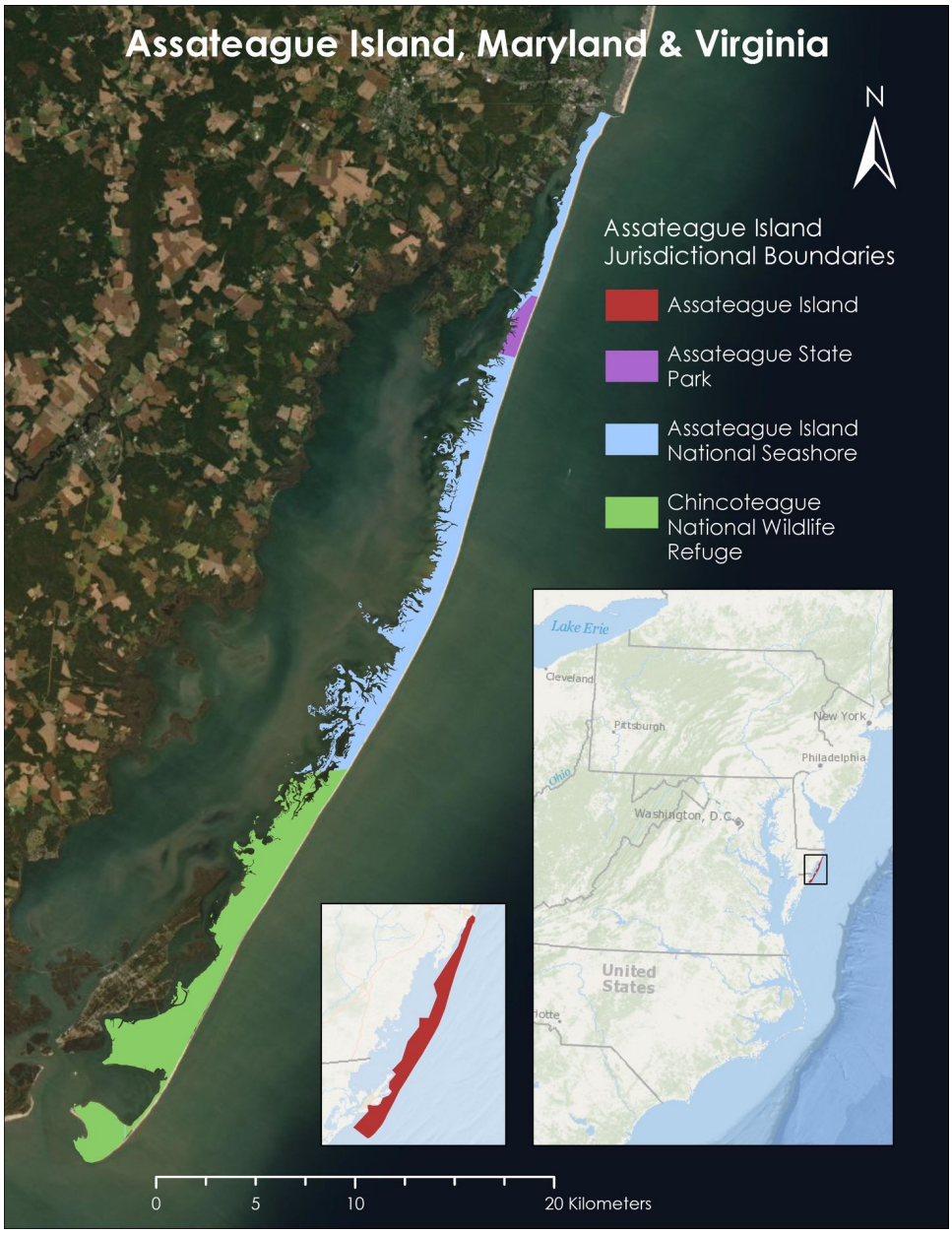

Figure 1. Study area: Assateague Island, Maryland and Virginia, USA. Base map source: Earthstar Geographics

Assateague Island, as shown in Figure 1, is situated off the coasts of Maryland and Virginia. The Assateague Island National Seashore (ASIS) encompasses the majority of the Maryland side and is managed by the National Park Service (NPS). Assateague Island State Park, managed by the Maryland Department of Natural Resources is also located in the northern portion. Meanwhile, the Virginia side of the island is the Chincoteague Wildlife Refuge, which is under the US Fish and Wildlife Service's jurisdiction. The entire island is approximately 60 km long (*Natural Features & Ecosystems,* 2015) and has a humid subtropical climate (Encyclopedia Britannica, n.d.). At present, Assateague Island's coast is classified as microtidal and wave-dominated and experiences a semidiurnal tidal cycle (Schupp, 2013).

As a barrier island, Assateague is constantly reshaped by natural processes and, more recently, anthropogenic modifications such as inlet stabilization. Assateague

Island's morphology is incredibly dynamic and driven by the effects of sediment supply, wind, storms, and sea level rise. On the ocean side, waves drive the longshore sediment transport, which trends net southwards and is estimated to carry between 115,000 and 214,000 m^3 of sediment per year. Meanwhile, the aeolian processes on land build and maintain dunes, carry sand to the island's center, and transport sediment to the Coastal Bays estuary. The region also experiences drastic changes like overwash events from hurricanes and northeasters (Schupp, 2013), and 30% of the ASIS shoreline is classified as highly vulnerable to sea level rise (Pendleton et al., 2004).

These unique coastal settings and dynamic process have led to Assateague Island serving as a home to various sensitive flora and fauna. Many species, like migrating shorebirds, rely on naturally disturbed areas for nesting and feeding (Schupp et al., 2013). The federally threatened piping plover (*Charadrius melodus*), for example, prefers minimally vegetated dunes to forage and nest, like those affected by overwash events (National Park Service, 2012). The threatened seabeach amaranth (*Amaranthus pumilus*) also inhabits these areas (Vegetation Classification, 2017). It is possible that the sensitive species of the island have been impacted by the sediment restoration project. To analyze the impacts of sediment bypassing operations on the sensitive habitats and geologic integrity of Assateague Island, our team used remote sensing to characterize historical trends in sediment transport and land cover change and model future land cover scenarios.

2.2 Project Partners & Objectives

NPS is dedicated to preserving the natural resources of National Parks; as such, they utilize natural or nature-based management strategies. One area where this applies is the sediment bypassing project, which was enacted by USACE. The operations are intended to mitigate the negative effects of the Ocean City inlet jetty system and protect Assateague's geologic integrity by restoring the natural sediment supply to the north end of the island (Zimmerman, 2004). However, USACE and NPS staff at ASIS were concerned with funding constraints for this project and any potential impacts on the sensitive species and geologic integrity of the island.

Our team partnered with USACE and NPS staff at ASIS, as well as collaborators within the Ocean and Coastal Resources Branch and Natural Resource Stewardship and Science Directorate of NPS. This project enabled USACE and NPS to understand the impact of sediment bypassing operations more fully and to make better informed management decisions regarding habitat protection. To accomplish these objectives, we used data from NASA Earth observations (EO), particularly Landsat 5 Thematic Mapper (TM), Landsat 7 Enhanced Thematic Mapper Plus (ETM+), Landsat 8 Operational Land Imager (OLI), and Sentinel-2 MultiSpectral Instrument (MSI) to create end products that reflect the changes in sediment transport from 2004 to 2020 and land cover from 2006 to 2018. These end products included time series maps of historical nearshore suspended sediment and land cover, as well as forecasted land cover change maps for 2021, 2031, and 2046.

3. Methodology

3.1 Data Acquisition

3.1.1 Sediment Transport

Our team acquired raster data of ocean color and turbidity to act as proxies for analyzing sediment transport. To do this, we used surface reflectance data from Sentinel-2 MSI Level-1C, Landsat 7 ETM+ Level-1TP, and Landsat 5 TM Level-1TP, which are summarized in Table 1. Winter turbidity and ocean color data from 2012 are absent due to Landsat 7's scan line corrector failure.

Table 1. Summary of satellites used for each sediment transport layer by year and season.

Year	**Summer**		**Winter**	
	Turbidity	*Ocean Color*	*Turbidity*	*Ocean Color*
2004	Landsat 5 TM	Landsat 5 TM	Landsat 5 TM	Landsat 5 TM
2006	Landsat 5 TM	Landsat 5 TM	Landsat 5 TM	Landsat 5 TM
2008	Landsat 5 TM	Landsat 5 TM	Landsat 5 TM	Landsat 5 TM
2010	Landsat 7 ETM+	Landsat 7 ETM+	Landsat 5 TM	Landsat 5 TM
2012	Landsat 7 ETM+	Landsat 7 ETM+	No data	No data
2014	Landsat 7 ETM+	Landsat 7 ETM+	Landsat 7 ETM+	Landsat 7 ETM+
2016	Sentinel-2 MSI	Sentinel-2 MSI	Sentinel-2 MSI	Sentinel-2 MSI
2018	Sentinel-2 MSI	Sentinel-2 MSI	Sentinel-2 MSI	Sentinel-2 MSI
2020	Sentinel-2 MSI	Sentinel-2 MSI	Sentinel-2 MSI	Sentinel-2 MSI

3.1.2 Historical Land Cover & Land Cover Forecasting

To analyze historical land cover change for Assateague Island, we accessed imagery from the Google Earth Engine (GEE) catalog for Landsat 8 OLI and TIRS Level 2, Collection 2, Tier 1 Surface Reflectance. We obtained Landsat 8 OLI imagery for October 1st, 2015 – September 30th, 2016, and October 2017 – September 2018. We also acquired USGS LiDAR-derived elevation data collected using the Experimental Advanced Airborne Research Lidar on 19 and 24 March 2010 from the NPS Integrated Resource Management Applications (IRMA) portal. This bare-earth digital elevation model (DEM) had a 2.5 m resolution.

Our ancillary data consisted of land cover products from the National Oceanic and Atmospheric Administration Coastal Change Analysis Program (NOAA C-CAP) and National Agriculture Imagery Program (NAIP) true color aerial imagery. We accessed NAIP imagery from the GEE catalog from August 1st, 2015, and June 26th, 2016. We obtained NOAA C-CAP data for 2006, 2010, and 2016 through the NOAA Data Access Viewer.

Our team used the IDRISI TerrSet Land Change Modeler (LCM) to forecast land cover in 2021, 2031, and 2046. For the model inputs, we acquired a 2006 NOAA C-CAP land cover product as the earlier image. We then used our 2018 historical land cover classification for the later image.

3.2 Data Processing

3.2.1 Sediment Transport

A previous DEVELOP team created the Optical Reef and Coastal Area Assessment (ORCAA) tool, which is a script in GEE used to process coastal remote sensing data

(Pippin et. al, 2019). To provide turbidity and ocean color outputs, ORCAA masked pixels with cloud cover and returned only surface reflectance values. The tool merged the individual data layers across a full year into a mosaic encompassing one calendar year of data. We then clipped each turbidity and ocean layer to our area of interest (AOI), which was the 2010 legal NPS boundary of Assateague Island.

We used the same turbidity equation as the creators of the ORCAA tool (Pippin et. al, 2019). The Nechad et al. equation utilizes red and near-infrared bands to compare marine water to Formazin, which is the turbidity calibration standard (Rice, 1976). Here, turbidity is measured in Formazin Nephelometric Units (FNUs):

$$\text{Turbidity (FNUs)} = (A_T * (\rho W * \textit{scale\_factor}) / (1 - ((\rho W * \textit{scale\_factor}) / C))) \quad (\textit{Equation 1})$$

where A_T (378.46) and C (0.19905) are calibration coefficients dependent on wavelength, and ρW at any wavelength is the water leaving reflectance, which is the red band in this case. The *scale_factor* is 0.0001. Further information on calibration coefficients and turbidity can be found in Pippin et al. (2019) and Nechad et al. (2009). Due to the temporal availability of Sentinel-2, we changed the ORCAA script to use Landsat 5 and 7. The functionalities of the scripts remained unchanged, and we only updated the band names and sensors.

3.2.2 Historical Land Cover

We decided to structure our land cover classes based on those found in NOAA C-CAP, as NPS had used it as a resource previously. We consolidated the nineteen C-CAP land cover classes found on Assateague Island into ten classes, which are shown in Table B2 located in Appendix B. In order to create training data for the Random Forest supervised land cover classification, we uploaded 2016 C-CAP data and NAIP imagery as GEE assets. We intended to create training data for both 2016 and 2018; however, the land cover types were not visually distinguishable using just NAIP imagery. This caused us to rely on NOAA C-CAP data, which was only available for 2016. We created one set of training data for 2016 and used it for both the 2016 and 2018 classifier because of this limitation. We found this to be a reasonable step because land cover changed minimally between 2010 and 2016 C-CAP datasets, with an overall agreement of 0.9996, suggesting that there was minimal land cover change between 2010 and 2016. Within GEE, we created fifteen training polygons for each land cover type. We converted these polygons to points in Esri ArcGIS Pro. To allow for independent validation of classifier results, we reserved 30% of this training data. We found this to be a reasonable step because land cover changed minimally between 2010 and 2016 C-CAP datasets, with an overall agreement of 99.96%, suggesting that there was minimal land cover change between 2010 and 2016.

We accessed Landsat 8 imagery for winter and summer seasons of 2016 and 2018 through GEE. After filtering imagery for scenes with less than five percent cloud cover, we created a composite image for each season consisting of the median values across the time span. We derived the following indices from these composite images: Normalized Difference Water Index, or NDWI (McFeeters, 1996), Normalized Difference Moisture Index, or NDMI (Hardisky et al., 1984),

Normalized Difference Vegetation Index, or NDVI (Rouse et al., 1974), and Tasseled Cap Transformation, or TCT (Baig et al., 2014). In Equations 2-7 below, *NIR* refers to the near infrared band, *SWIR1* is the first short-wave infrared band, *SWIR2* is the second short-wave infrared band, and *Green*, *Red*, and *Blue* are the color bands.

$$NDWI = (¿ - NIR)/(¿ - NIR) \quad (2)$$

$$NDMI = (NIR - SWIR\,1)/(NIR + SWIR\,1) \quad (3)$$

$$NDVI = (NIR - ¿)/(NIR + ¿) \quad (4)$$

$$TCT\,(Wetness) = (¿ * 0.1511) + (¿ * 0.1973) + (¿ * 0.3283) + ¿ \quad (5)$$
$$(NIR * 0.3404) + (SWIR\,1 * -0.7117) + (SWIR\,2 * -0.4559)$$

$$TCT\,(Greenness) = (¿ * -0.2941) + (¿ * -0.243) + (¿ * -0.5424) + ¿ \quad (6)$$
$$(NIR * 0.7276) + (SWIR\,1 * 0.0713) + (SWIR\,2 * -0.1608)$$

$$TCT\,(Brightness) = (¿ * 0.3029) + (¿ * 0.2786) + (¿ * 0.4733) + ¿ \quad (7)$$
$$(NIR * 0.5599) + (SWIR\,1 * 0.508) + ¿\ (SWIR\,2 * 0.1872)$$

3.2.3 Land Cover Forecasting

To produce homogeneous land cover inputs for the creation of our forecast maps, we used the Harmonize interface within the LCM software. This allowed our team to process both the 2016 NOAA C-CAP data as well as our 2018 land cover classification. This was a necessary step within our forecast workflow, as the LCM software requires input layers to have the same extent, projection, background areas, background values, and legend in order to calculate the changes between them. Therefore, these layers were reclassified within the interface to allow progression of the forecast methodology.

3.3 Data Analysis

3.3.1 Sediment Transport

To analyze ocean color and turbidity data collected from ORCAA, we used the tool's built-in time series chart function to generate graphs of the two variables over time. This time series chart function allows the user to plot daily or monthly averages of ocean color or turbidity over the selected area on a line graph (Pippin et al., 2019). We analyzed ocean color and turbidity during even years (2004, 2006, … 2020) and split each analysis year into 'summer' (April-September) and 'winter' (October-March). This was to account for seasonal changes in wave energy, beach slope, and beach volume (Shepard, 1950; Aubrey, 1979).

3.3.2 Historical Land Cover

We performed a Random Forest supervised land cover classification to produce land cover classifications of the study area for 2016 and 2018. Random Forest (RF) is a machine-learning algorithm which learns to identify land cover types from satellite imagery. To conduct the RF land cover classification, we adapted three GEE scripts created by the Fall 2020 Southern Colorado Disasters DEVELOP team

in Fall 2020 (Cunningham et. al, 2020). We merged Landsat 8 bands 1-7 and surface temperature band 10, a 2010 DEM, and indices for NDWI, NDMI, NDVI, and TCT into a single multiband image. We then sampled this input image stack at each training point, attaching attributes to each point. Using these sampled points, we trained a Random Forest classifier. We fed our input image stack into this trained classifier and ran it using a bag fraction of 0.6 and 1000 iterations per run, then repeated this process for 2018.

3.3.3 Land Cover Forecasting

LCM, or the modeling system integrated within TerrSet that we used to forecast land cover, operates and predicts future land cover by detecting patterns of historical land cover change. The modeler then utilizes those patterns to forecast changes that are most likely to occur based on trends identified during the pattern evaluation. For our analysis, we created forecast maps that projected out to the years of 2021, 2031, and 2046. For our methodology, we used the Change Analysis tool within the modeler to identify land cover change patterns between 2006-2018, and then we created change analysis maps identifying the various land cover transition types. With the transition types found by the change analysis, we created transition potentials, which are indicators of the likelihood for a specific land cover type to transition into another type. Last, we used a stochastic model known as a Markov Chain to forecast future land cover for Assateague Island in the desired years of 2021, 2031, and 2046.

4. Results & Discussion

4.1 Analysis of Results

4.1.1 Sediment Transport

Overall, we saw trends in turbidity on all sides of the island that varied by season. We generally saw higher turbidity on the western bayside of the island. In the summer months, we observed overall higher turbidity on the ocean-facing northern and southern ends, but not in the center portion of the island. In the winter, we saw higher levels of turbidity in the middle of the island, which is likely due to winter storms. Pixels close to land had the largest turbidity values, and turbidity values decreased quickly as distance from the shore increased on the ocean side. Plumes of sediment were the most visible on the bay side and in newer ocean color imagery. We also saw evidence of longshore transport and deposition in the growth of the southern portion of the island, which is where sediment has been accumulating historically. These seasonal, bi-yearly layers were useful for showing where turbid waters and plumes exist, but not the specifics on type and quantity of any matter suspended in the water column. Maps of seasonal ocean color and turbidity can be found in Appendices A1-A4, and charts of turbidity from individual sediment bypassing events can be found in Appendix A5. Figure 2 shows the results of one such case study, showcasing a time series chart along with maps of turbidity.

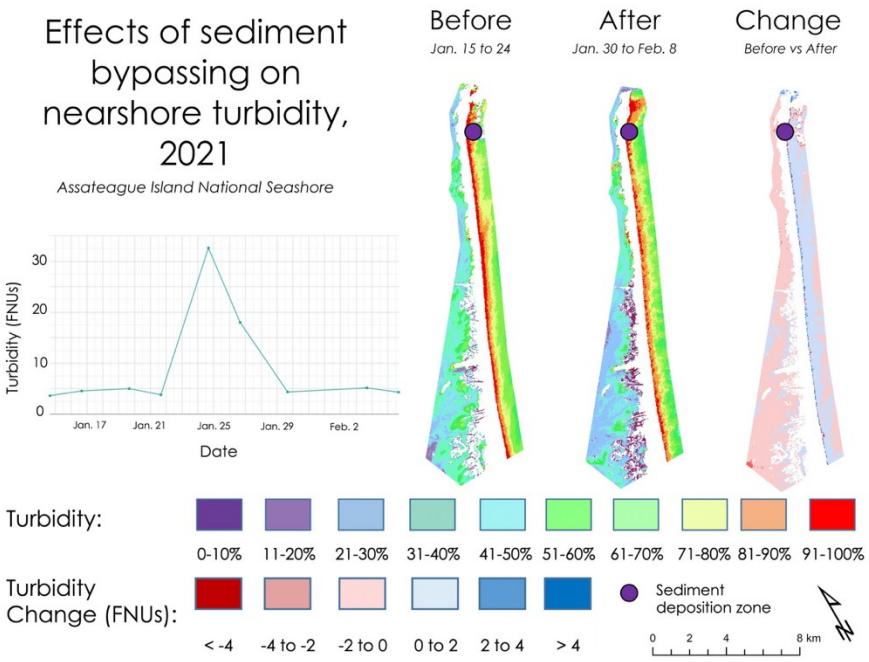

Figure 2. Effects of a January 2021 sediment bypassing event on nearshore turbidity. Areas shaded in blue in the change map show increases in turbidity post-bypassing event.

Sediment bypassing events can be clearly seen through NASA and ESA Earth observations. The chart in Figure 2 shows the sharp change in nearshore turbidity during the deposition events as compared to before and after a sediment bypassing event in January of 2021. It's possible that other factors like the weather influenced these spikes in turbidity. Additional time series charts of turbidity from 2016-2020 can be seen in Figure A5 shown in Appendix A. Similar spikes in turbidity can be seen in these additional charts as well, where the date ranges of the sediment bypassing events themselves are shown, along with ten days before and ten days after the deposition.

4.1.2 Historical Land Cover

By analyzing the results of our land cover classification, we found that the 2018 Random Forest land cover classification was highly accurate, with an overall accuracy of 98% based on an independent validation. We performed this independent validation by creating an agreement matrix comparing the 2018 classifier output and the reserved 30% of the training data. The largest net decreases in land cover between 2006 and 2018 were in barren land and open water, where barren land had a decrease of approximately 10 square kilometers, while open water had a decrease of approximately 7 square kilometers. Meanwhile, the largest net increase in land cover between 2006 and 2018 was in unconsolidated shore, with an increase of approximately 9 square kilometers. There was minimal net change in wetland land cover categories, as shown in Table 2. In addition, to visualize land cover change across the island over the twelve years, we made a set of maps showing land cover by class type (Figure B1, Appendix B) and showing land cover gains and losses by category between 2006 and 2018 (Figures B2 and B3, Appendix B)

Table 2. Land cover change from 2006 to 2018.

Land Cover Class	Net Change (km^2)	Gain (km^2)	Loss (km^2)
Developed	3.52	3.87	-0.35
Grassland	2.38	2.79	-0.41
Forest	0.39	3.35	-2.95
Shrub	2.15	3.74	-1.59
Palustrine Forested Wetland	-0.22	5.06	-5.27
Palustrine Emergent/Shrub Wetland, Aquatic Bed	1.63	3.56	-2.93
Estuarine Emergent/Shrub Wetland	-1.14	8.67	-9.81
Unconsolidated Shore	8.76	10.42	-1.66
Barren Land	-9.86	0.58	-10.44
Open Water	-6.62	3.69	-10.31

Further transitions can be seen in the numerical outputs calculated through agreement matrices, which are shown in Table B1 in Appendix B. This table shows the land cover transitions from 2006 to 2018. The columns represent land cover in 2006 while the rows represent land cover in 2018. Looking specifically at the "forest" land cover type, 39% of the forest that existed in 2006 remained as forest in 2018. The most frequent transition of the forest land cover class was to palustrine forested wetland; therefore 36% of what was forest in 2006 became palustrine forested wetland in the time period between 2006 and 2018. The three land cover types with the highest level of persistence from 2006 to 2018 were open water, unconsolidated shore, and estuarine emergent/shrub wetland, with persistence rates of 89%, 72%, and 67%, respectively (Table B1, Appendix B). Land cover classes with the highest levels of change were palustrine emergent/shrub wetland, aquatic bed, shrub, and developed, with change rates of 80%, 68%, and 67%, respectively (Table B1, Appendix B).

4.1.3 Land Cover Forecasting

We used the IDRISI TerrSet Land Change Modeler (LCM) software to produce our land cover forecast maps. The LCM works by detecting patterns seen in previous land cover change and then using those patterns to predict future land cover changes based on the trends seen historically. The input historical land cover that was used in the LCM came from reclassified 2006 NOAA C-CAP data as well as the 2018 historical land cover classification made by our team. When visually interpreting the forecast maps, we saw striping in the upper portion of the 2031 and 2046 predictions, which is an abnormal output of the LCM. Therefore, these maps are most likely unreliable, and we advise this be kept in mind, should they be used as a tool for interpretation of future habitat suitability.

The numerical outputs of our forecasts are available in Tables C1, C2, and C3 within Appendix C. Looking at the 2021 forecast (Table C1), the largest predicted increase was for developed land. This predicted increase could be due to development trends seen within the 2006 and 2018 timeline, which the LCM then used as a trend in its predictions. This increase could also be due to the absence of development changes that were exempted. The exemption of these development changes was made by our team due to their unlikely nature, as the LCM was

predicting developed areas to transition into land cover types such as forest, unconsolidated shore, and wetlands, which did not seem likely. Following developed land, the second largest increase in the 2021 forecast was unconsolidated shore, with a predicted gain of approximately 1.7 square kilometers. Meanwhile, in the 2031 forecast the foremost greatest increase predicted was unconsolidated shore with a gain of approximately 6 square kilometers. Lastly, looking at the 2046 forecast, unconsolidated shore was again predicted to increase the most compared to other land cover types at an estimated 11 square kilometers of predicted gain. Also, in the 2046 forecast, a projected decrease of open water was observed at a predicted decrease of approximately 12 square kilometers in area. While these trends may make sense when considering the sediment bypassing operations and observing the accretion seen on the southern side of the island, we would like to acknowledge again that these results are most likely unreliable, due to the striping output seen visually from the maps shown below in Figure 3.

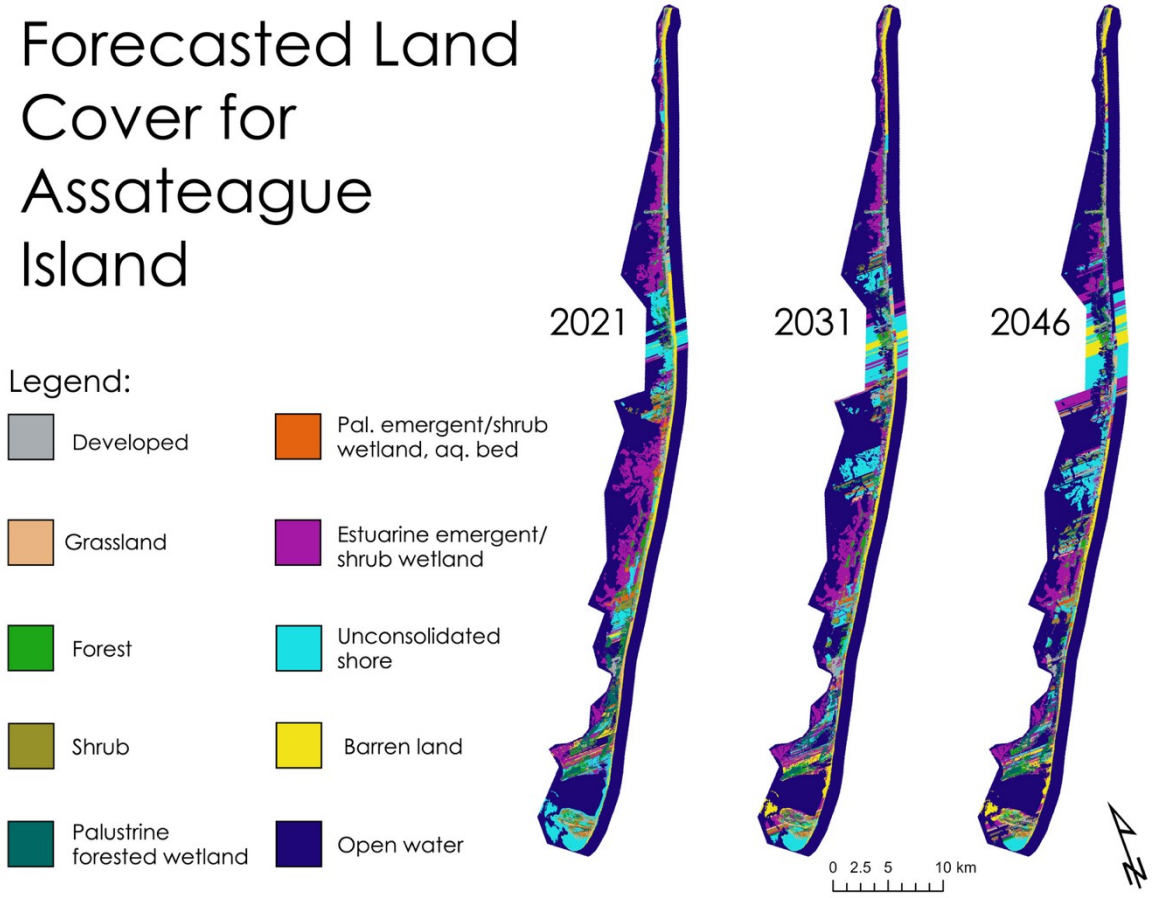

Figure 3. Land cover forecasts of 2021, 2031, and 2046 based on historical land cover change between 2006 and 2018.

4.2 Errors and Uncertainties

Overall, our methods and results relied on several assumptions that must be kept in mind for our interpretations. For example, in our turbidity analysis, the spatial resolution of 30 meters may have been too coarse to see smaller-scale plumes of sediment. Additionally, our turbidity layers could also be showing suspended

organic matter as well as sediment, which could give a false sense of high turbidity.

In regard to our land cover classification, our raster layers often had multiple landcover types per pixel that were not visually distinguishable from reference imagery. Without ground-truthing, this introduced inherent uncertainty within the classification. Furthermore, we condensed similar landcover classes from the 2016 NOAA C-CAP data for our historical classification. For example, we combined multiple different wetland types into a single 'wetland' category, as shown in Appendix C4. This potentially introduced error by making classes that are less spectrally unique, less accurate, or overly simplified than the original NOAA C-CAP classes.

For landcover forecasting, we did not use explanatory variables to account for dynamic drivers of change. Examples of explanatory variables that would have been used include NDWI, NDVI, and elevation. However, implementing these variables was not practical within our time constraints, and there were implicit complications associated with modeling dynamic, explanatory variables. Therefore, we decided to exclude dynamic variables and instead utilized a single static variable within our stochastic change model. This variable was a land cover policy input, which was held static because it was assumed that the land cover policy held by NPS would not be altered significantly in the near future. These potential errors and uncertainties could be used to inform future research and provide room for future work to be done.

4.3 Future Work

Additional analyses of nearshore sediment transport, habitat classification, and habitat forecasting could be done to build upon the work presented here. We would suggest further case studies for analyzing changes in suspended sediment pre- and post-deposition to better characterize the process of sediment transport in Assateague's nearshore. Different remote sensing methods could also be employed to better distinguish sediment from other factors influencing turbidity. A volumetric change analysis would provide a method for analyzing the quantity, location, and movement of sediment over time in relation to sediment bypassing operations. These change detections could be done using cross-shore transects, LiDAR, or aerial imagery to create surfaces at multiple points in time, then subtract them to determine regions of change. Also, the spatial resolution of Landsat 7/8, 30 m, could be considered coarse, and for a more accurate land cover classification, we recommend using a finer resolution dataset like aerial or Planet Labs satellite imagery. Additionally, to improve our landcover classification, we would suggest ground truthing, forecasting at different timescales, including explanatory variables, and adding more inputs such as canopy height to the classifier. For land cover forecasting, alternative analyses could be performed by selecting different sub-model structures within the LCM. Also, by implementing the use of dynamic drivers of change and explanatory variables, more reliable forecast could potentially be produced. Finally, it could be useful to perform a habitat suitability analysis for sensitive species like the piping plover and seabeach amaranth.

5. Conclusions

Overall, by working with our partners at NPS and USACE, our team provided a series of historical change maps for sediment transport and land cover, plus land cover change models for 10 and 25 years into the future. The ORCAA tool provided

a successful avenue for visualizing trends in ocean color and turbidity. We saw seasonal trends and overall growth on the south side of the island. However, we were unable to quantify sediment movement nor distinguish what matter is suspended in the water column. For our landcover work, we observed trends like a decrease in 'open water' and increase in 'unconsolidated shore' on the island between 2006 and 2018. We used these landcover classifications to forecast landcover to 2021, 2031, and 2046. While there is room for future work, our results helped our partners review the efficiency of sediment bypassing operations and their impacts on Assateague's geology and ecology. With our help, they were also able to make better-informed decisions for park management strategies to protect sensitive species on the island.

6. Acknowledgments

We would like to thank the following individuals for their incredible assistance with our project:

- Brandy Nisbet-Wilcox (Fellow, NASA DEVELOP Program, Idaho)
- Keith Weber (Science Advisor, Idaho State University)
- Dr. Kenton Ross (Science Advisor, NASA Langley Research Center)
- Bill Hulslander (Park Manager, Assateague Island National Seashore)
- Catherine Johnson (Coastal Ecologist, Northeast Region)
- Justin Callahan (Project Manager, United States Army Corps of Engineers)
- Monique LaFrance Bartley (Marine Ecologist, Ocean and Coastal Resources Branch)
- Dave Brinker (Regional Ecologist, Maryland Department of Natural Resources)
- Hayley Pippin (Geoinformatics Fellow, NASA DEVELOP Program)
- Scott Cunningham, Audrey Colley, Camille Blose, and David Keyes (DEVELOP Fall 2020 Southern Colorado Disasters Team)
- Arbyn Olarte, Roxana Pilot, Vanessa Valenti, and Hayley Pippin (DEVELOP Fall 2019 Belize and Honduras Water Resources II Team)

This material contains modified Copernicus Sentinel data (2021), processed by ESA.

Any opinions, findings, and conclusions or recommendations expressed in this material are those of the author(s) and do not necessarily reflect the views of the National Aeronautics and Space Administration.

This material is based upon work supported by NASA through contract NNL16AA05C.

7. Glossary

Acronyms

AOI – Area of Interest
ASIS – Assateague Island National Seashore
C-CAP – Coastal Change Analysis Program
DEM – Digital Elevation Model
DEVELOP – Digital Earth Virtual Environment and Learning Outreach Project
FNU – Formazin Nephelometric Units
GEE – Google Earth Engine
GIS – Geographic Information Systems; alternatively Geographic Information Science

IRMA – Integrated Resource Management Applications, a portal for accessing National Park Service data
LCM – Land Change Modeler
LiDAR – Light Detection and Ranging
NASA – National Aeronautics and Space Administration
NDMI – Normalized Difference Moisture Index
NDVI – Normalized Difference Vegetation Index
NDWI – Normalized Difference Water Index
NOAA – National Oceanic and Atmospheric Administration
NPS – National Park Service
ORCAA – Optical Reef and Coastal Area Assessment
TCT – Tasseled Cap Transformation
USACE – United States Army Corps of Engineers
USGS – United States Geological Survey

Satellites and Instruments
Earth observations (EO) – Satellites and sensors that collect information about the Earth's physical, chemical, and biological systems over space and time
Landsat 5 TM – Landsat 5 Thematic Mapper; the fifth satellite of the NASA Landsat program, launched in 1984, carrying multispectral sensors such as the TM instrument
Landsat 7 ETM+ – Landsat 7 Enhanced Thematic Mapper Plus; the seventh satellite of the NASA Landsat program, launched in 1999, carrying multispectral sensors such as the ETM+ instrument
Landsat 8 OLI – Landsat 8 Operational Land Imager; the eighth satellite of the NASA Landsat program, launched in 2013, carrying multispectral sensors such as the OLI instrument
Sentinel-2 MSI – Sentinel-2 MultiSpectral Instrument; the second satellite of the European Space Agency's Copernicus Sentinel Programme, launched in 2015, carrying remote sensing instruments like the MSI

Scientific Vocabulary
Aeolian – Relating to wind activity and its impact on earth's materials and surface landforms
Anthropogenic – Originating from human activity
Barrier island – An island and dune system situated parallel lengthwise to the mainland coast; particularly long and narrow on microtidal coasts such as for Assateague Island
Dune – Low mound or ridge of sand deposited and shaped by wind
Estuary – Seaward end or tidal mouth of a river characterized by brackish water and a mixed energy environment of river currents, waves, and tidal influence
Humid subtropical – Refers to a climate characterized by cold to mild winters and hot and humid summers
Littoral zone – Coastal zone extending from the mean high tide line to the end of the continental shelf and supporting benthic vegetation
Longshore – Along the shore; in this case referring to the natural, wave-driven movement of sediment net parallel to the shoreline
Markov chain – Model of randomly sequenced events which builds a chain of relatively referenced random events
Microtidal – Refers to a coast with a mean tidal range of less than two meters
Nearshore – Coastal area containing shallow waters extending beyond the mean low tide line
Northeaster – Storm with winds blowing from the northeast

Overwash – Event where water and sediment overflow a barrier island during a storm or high tide, which moves sediment and facilitates the migration of an island closer to the mainland
Sediment bypass – Transport of sediment beyond a fixed geographical location, typically referring to natural transport processes; for the purpose of this project, sediment bypass is used to describe the sediment dredging and subsequent deposition along the island's littoral zone as performed by the United States Army Corps of Engineers as part of Assateague Island's north end restoration project
Semidiurnal – Refers to a tidal cycle consisting of two approximately equal high and low tides per lunar day
Tidal range – Difference in height between mean high tide and mean low tide of a particular area
Wave-dominated – Refers to a depositional coast where the driving factors of geomorphology and sediment transport are consistent, relatively large waves and their associated wave-generated currents

8. References

Aubrey, D. (1979). Seasonal patterns of onshore/offshore sediment movement. *Journal of Geophysical Research: Oceans*, *84*(C10), 6347–6354. https://doi.org/10.1029/JC084iC10p06347.

Baig, M. H. A., Zhang, L., Shuai, T., & Tong, Q. (2014). Derivation of a tasseled cap transformation based on Landsat 8 at-satellite reflectance. *Remote Sensing Letters*, *5*(5), 423-431.

Coastal Change Analysis Program Land Cover Classifications. (2021). National Oceanic and Atmospheric Administration Office for Coastal Management. https://coast.noaa.gov/data/digitalcoast/pdf/ccap-class-scheme-regional.pdf.

Cunningham, S., Keyes, D., Blose, C., & Colley A. (2020). *Using NASA Observations to Map Aspen Extent and Recovery Due to Wildfire*. Unpublished manuscript. Retrieved from https://www.devpedia.developexchange.com/dp/index.php?title=Southern_Colorado_Disasters_CO_Fall_2020.

Encyclopedia Britannica. (n.d.). Climate of Maryland. In *Britannica.com encyclopedia*. Retrieved June 28, 2021, from https://www.britannica.com/place/Maryland-state/Climate.

Encyclopedia Britannica. (n.d.). Climate of Virginia. In *Britannica.com encyclopedia*. Retrieved June 28, 2021, from https://www.britannica.com/place/Virginia-state/Climate.

Hardisky, M. A., F. C. Daiber, C. T. Roman, and V. Klemas. (1984). Remote sensing of biomass and annual net aerial primary productivity of a salt marsh. Remote Sensing of Environment 16:91–106.

McFeeters, S. K. (1996). The use of the Normalized Difference Water Index (NDWI) in the delineation of open water features. *International Journal of Remote Sensing*, *17*(7), 1425-1432.

National Park Service (2012). *Piping Plover (Charadrius melodus). Resource Management Brief NPS/ASIS.* Assateague Island National Seashore, Berlin, Maryland. http://npshistory.com/publications/asis/briefs/plover-2012.pdf.

National Park Service (2017). *Abbreviated Final General Management Plan and Environmental Impact Statement.* Assateague Island National Seashore, Berlin, Maryland. http://npshistory.com/publications/asis/final-gmp-2017.pdf.

Natural Features & Ecosystems. (2015, February 26). Assateague Island National Seashore, National Park Service. Retrieved June 30, 2021, from https://www.nps.gov/asis/learn/nature/naturalfeaturesandecosystems.htm.

Nechad, B., Ruddick, K. G., Neukermans, G. (2009). Calibration and validation of a generic multisensor algorithm for mapping of turbidity in coastal waters. *Proceedings Volume 7473, Remote Sensing of the Ocean, Sea Ice, and Large Water Regions 2009, 7473*. https://doi.org/10.1117/12.830700

Pendleton, E. A., Williams, S. J., & Thieler, E. R. (2004). *Coastal Vulnerability Assessment of Assateague Island National Seashore (ASIS) to Sea-level Rise*. *USGS Open-File Report 2004-1020.* United States Geological Survey, Woods Hole, Massachusetts. https://pubs.usgs.gov/of/2004/1020/images/pdf/asis.pdf.

Pippin, H., Valenti, V., Olarte, A., & Pilot, R. (2019). *Developing a Google Earth Engine Dashboard for Assessing Coastal Water Quality in the Belize and Honduras Barrier Reefs to Identify Adequate Waste Control and Inform Coastal Resource Monitoring and Management*. Unpublished manuscript. Retrieved from https://www.devpedia.developexchange.com/dp/index.php?title=Belize_%26_Honduras_Water_Resources_II_JPL_Fall_2019.

Rice, E.W. (1976). The preparation of formazin standards for nephelometry. *Analytica Chimica Acta*, *87*(1), 251-253. https://doi.org/10.1016/S0003-2670(01)83146-9

Rouse, J. W., Haas, R. H., Schell, J. A., & Deering, D. W. (1974). Monitoring vegetation systems in the Great Plains with ERTS. *NASA Special Publication*, *351*(1974), 309.

Schupp, C. (2013). *Assateague Island National Seashore: geologic resources inventory report. Natural resource report NPS/NRSS/GRD/NRR—2013/708.* National Park Service, Fort Collins, Colorado. http://npshistory.com/publications/asis/nrr-2013-708.pdf.

Schupp, C. A., Winn, N. T., Pearl, T. L., Kumer, J. P., Carruthers, T. J. B., & Zimmerman, C. S. (2013). Restoration of overwash processes creates piping plover (Charadrius melodus) habitat on a barrier island (Assateague Island, Maryland). *Estuarine, Coastal and Shelf Science*, *116*, 11–20. https://doi.org/10.1016/j.ecss.2012.07.003.

Shepard, F. P. (1950). Beach cycles in southern California. U.S. Army Beach Erosion Board Tech. Memo. 20, 26 pp.

Vegetation Classification and Mapping of Assateague Island National Seashore. (2017, April). Assateague Island National Seashore, National Park Service. Retrieved June 30, 2021.

Zimmerman, C. (2004). *Executive Summary – North End Restoration.* Assateague Island National Seashore, Resource Management Division, Berlin, Maryland.

9. Appendices

Appendix A: Sediment Transport

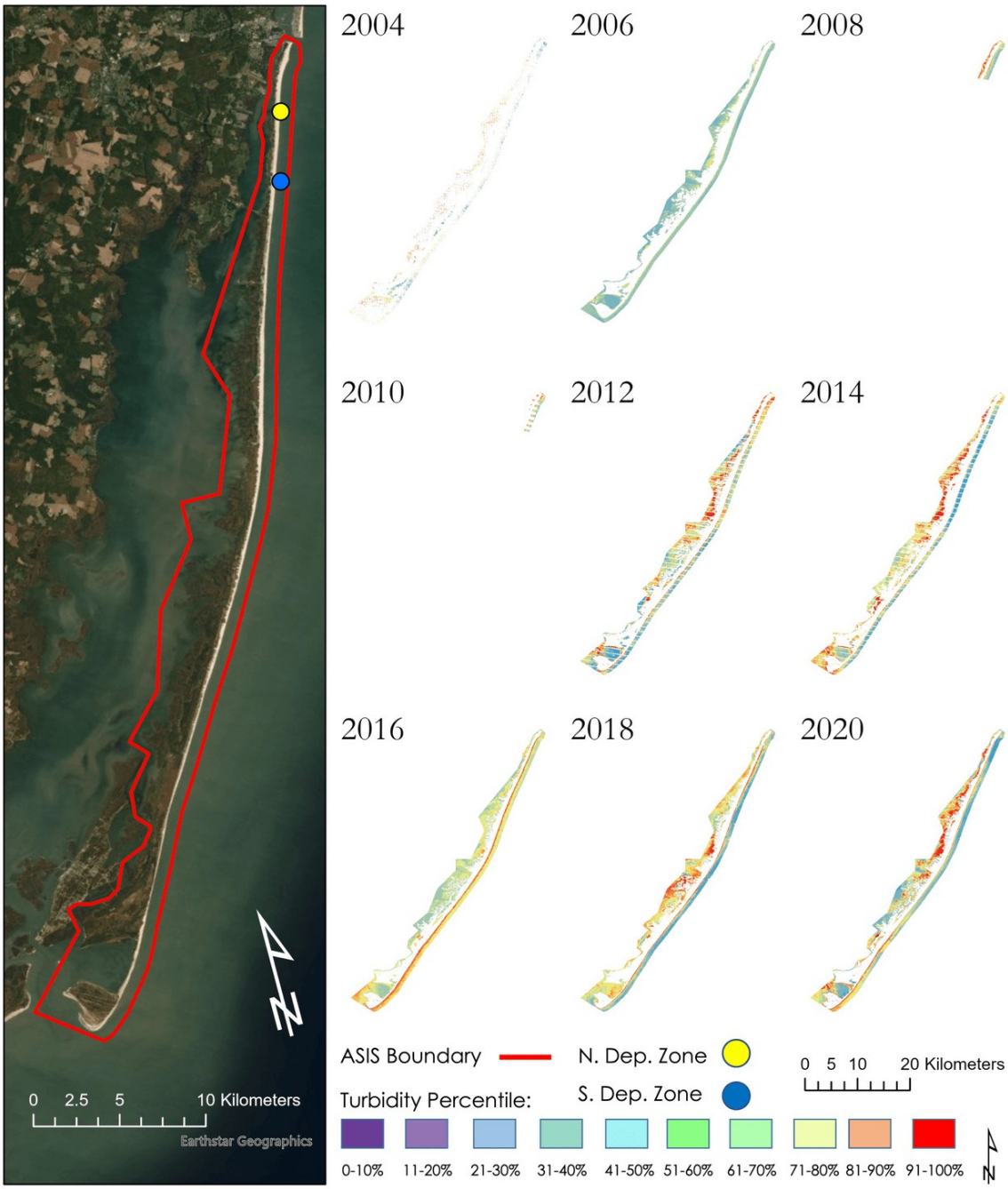

Figure A1. Time series maps of nearshore turbidity for the summer months of even years between 2004 and 2020 derived from Landsat 5 TM, Landsat 7 ETM+, and Sentinel-2 MSI surface reflectance data. Explanations of trends in seasonal turbidity can be found in Section 4.1.1.

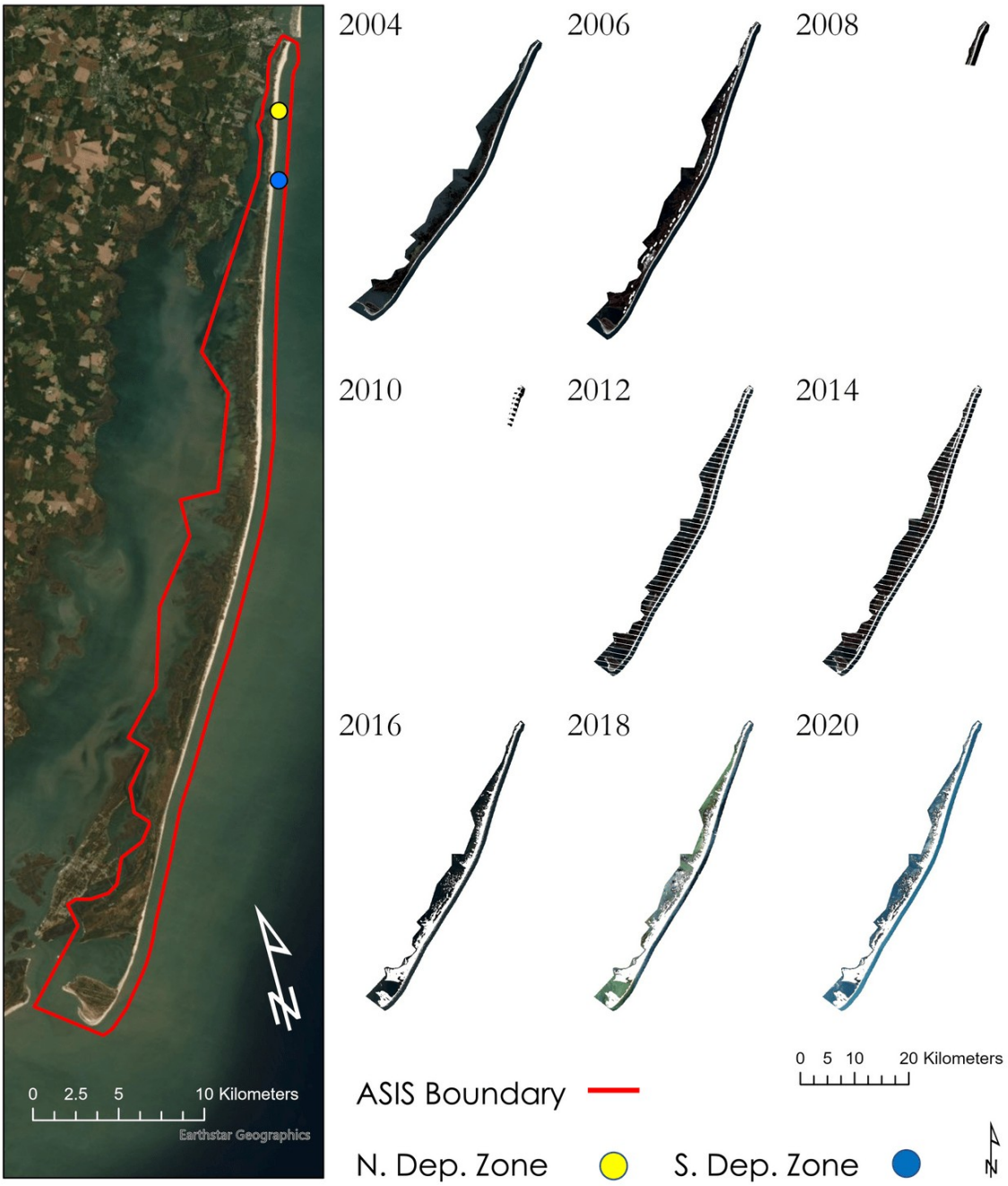

Figure A2. Time series maps of nearshore ocean color for the summer months of even years between 2004 and 2020 derived from Landsat 5 TM, Landsat 7 ETM+, and Sentinel-2 MSI surface reflectance data. Explanations of trends in seasonal ocean color can be found in Section 4.1.1.

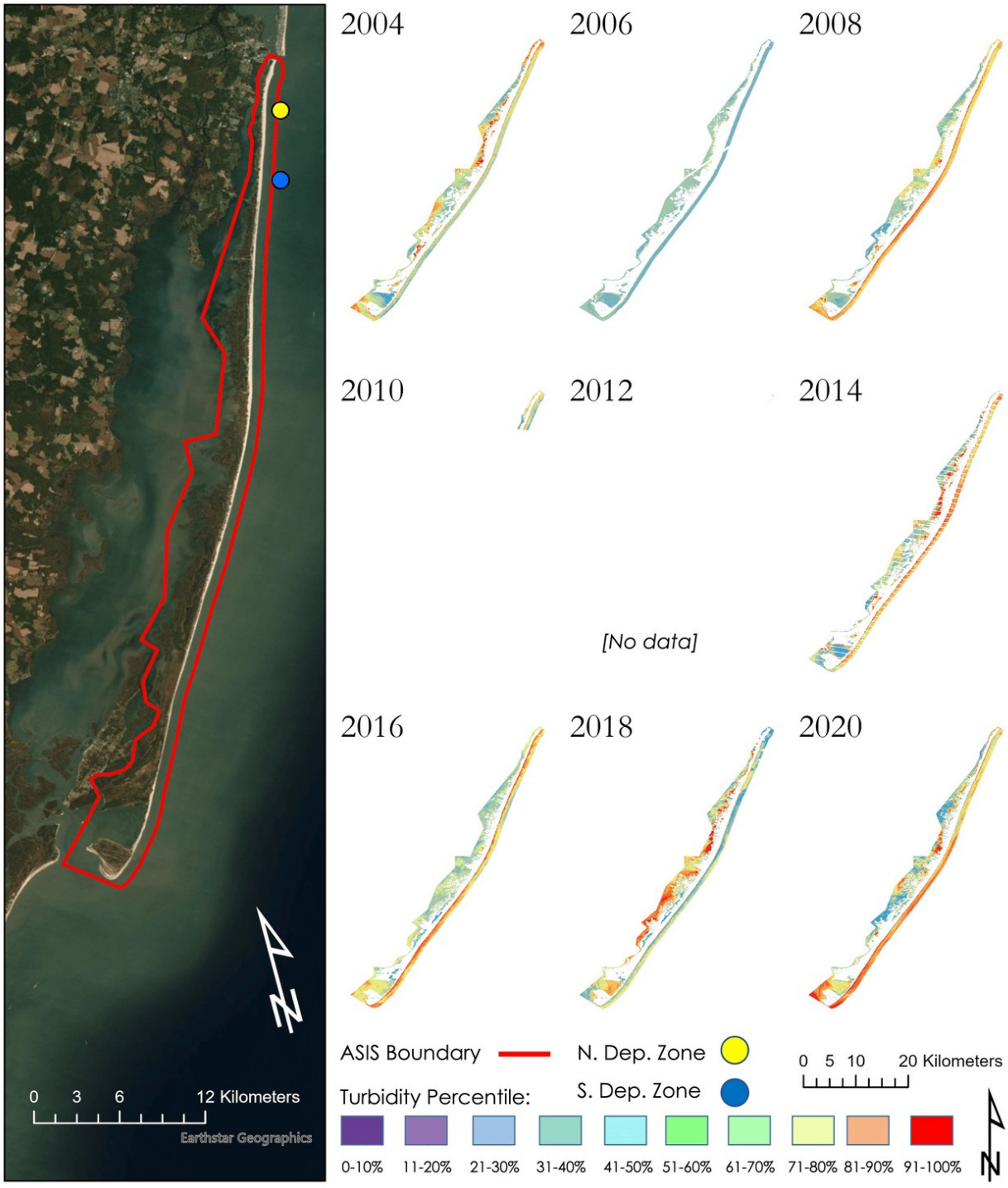

Figure A3. Time series maps of nearshore turbidity for the winter months of even years between 2004 and 2020 derived from Landsat 5 TM, Landsat 7 ETM+, and Sentinel-2 MSI surface reflectance data. Explanations of trends in seasonal turbidity can be found in Section 4.1.1.

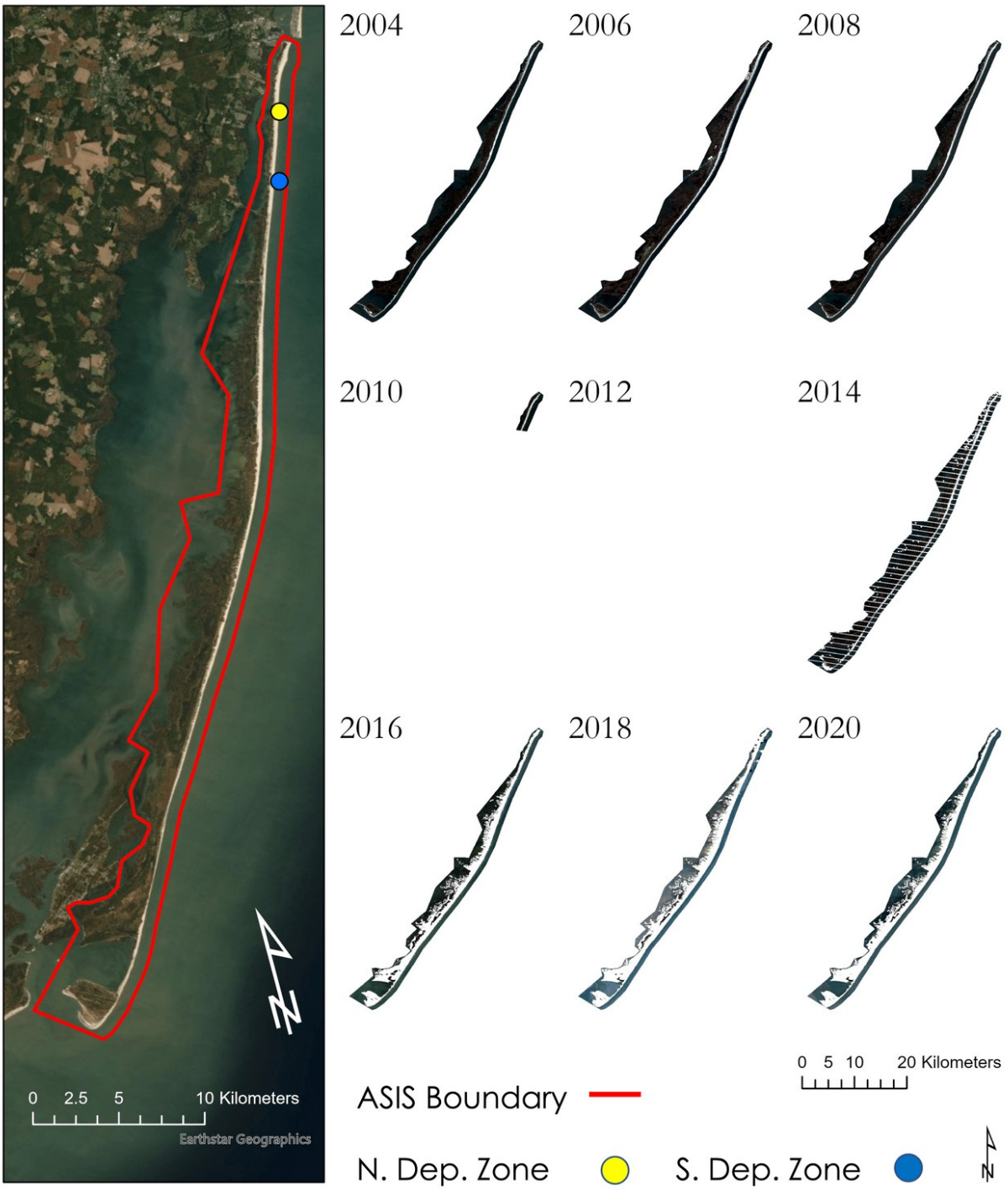

Figure A4. Time series maps of nearshore ocean color for the winter months of even years between 2004 and 2020 derived from Landsat 5 TM, Landsat 7 ETM+, and Sentinel-2 MSI surface reflectance data. Explanations of trends in seasonal ocean color can be found in Section 4.1.1.

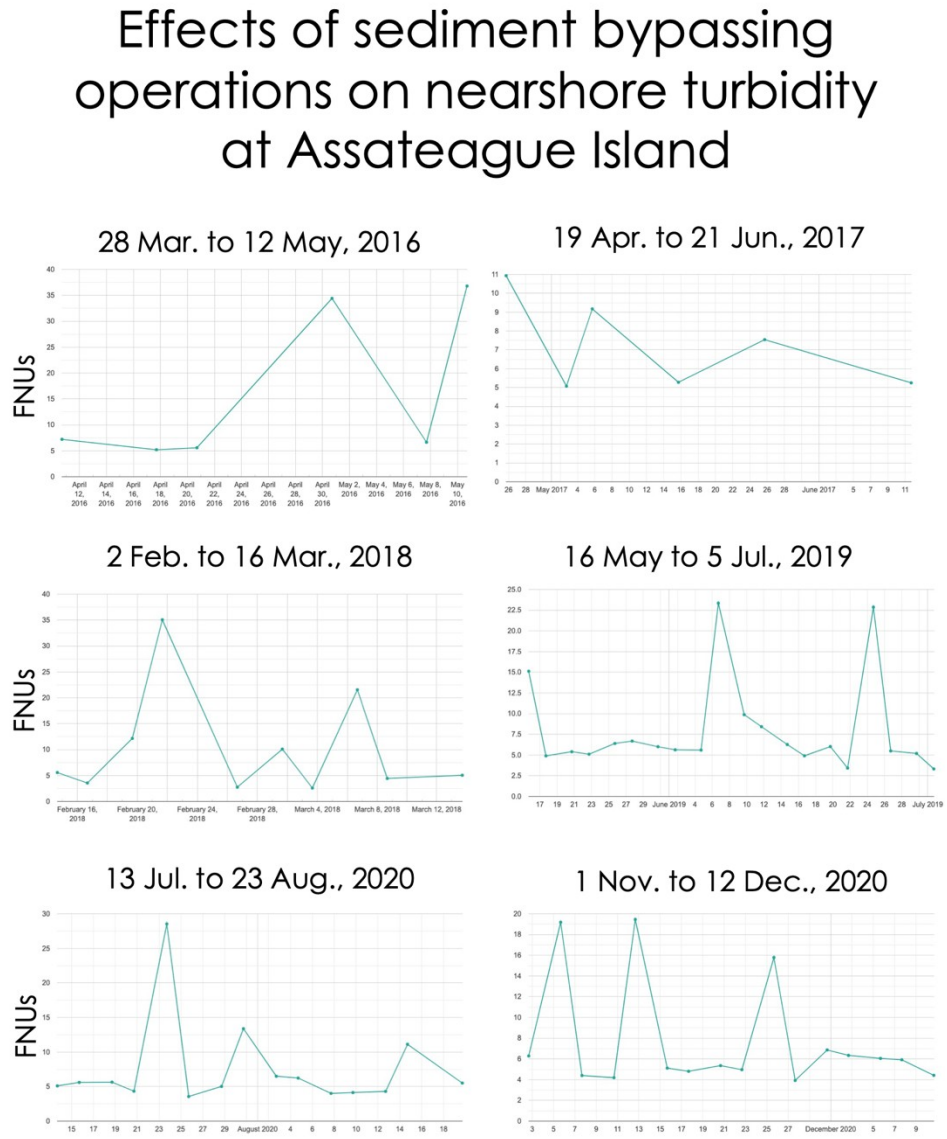

Figure A5. Time series turbidity charts of sediment bypassing events (+/- 10 days) derived from Sentinel-2 using the ORCAA tool on GEE from 2016-2020. These charts show increases in overall turbidity when sediment bypassing events are happening, showing they can be identified using Earth observations.

Appendix B: Landcover Classification

Table B1. Percent of land cover change from 2006 to 2018, where blue highlighting exhibits the percentage of land cover types remaining the same and yellow highlighting displays the greatest amount of transition from one land cover type into another. The numbers in the first row refer to different land cover types where 1 is developed land, 2 is grassland, 3 is forest, 4 is shrub, 5 is palustrine forested wetland (PFW), 6 is palustrine emergent shrub/wetland, aquatic bed (PESWAB), 7 is estuarine emergent shrub/wetland (EESW), 8 is unconsolidated shore, 9 is barren land, and 10 is open water.

	1	**2**	**3**	**4**	**5**	**6**	**7**	**8**	**9**	**10**
Developed	33%	5%	2%	6%	2%	3%	1%	1%	15%	0%
Grassland	1%	53%	1%	1%	1%	2%	1%	1%	13%	0%
Forest	9%	3%	39%	16%	16%	13%	2%	0%	1%	0%
Shrub	6%	7%	11%	32%	6%	8%	3%	1%	7%	0%
PFW	8%	3%	36%	21%	46%	23%	5%	1%	1%	0%
PESWAB	6%	7%	6%	10%	12%	20%	3%	3%	3%	0%
EESW	9%	1%	3%	11%	10%	11%	67%	5%	1%	5%
Unconsol-idated Shore	24%	10%	2%	3%	7%	19%	14%	72%	7%	3%
Barren Land	2%	10%	0%	0%	0%	1%	1%	3%	42%	0%
Open Water	2%	0%	0%	0%	0%	0%	4%	12%	10%	89%

Table B2. Consolidation process of the NOAA C-CAP Regional Land Cover Classification Scheme (*Coastal Change Analysis Program Land Cover Classifications*, 2021).

NOAA C-CAP Land Cover Class	New Class	Color
Developed, low intensity Developed, medium intensity Developed, high intensity Developed, open space	Developed	
Grassland, Cultivated	Grassland	
Deciduous forest, Evergreen forest, Mixed forest	Forest	
Scrub/Shrub	Shrub	
Palustrine forested wetland	Palustrine forested wetland	
Palustrine emergent wetland Palustrine scrub/shrub wetland Aquatic bed	Palustrine emergent/shrub Wetland, aquatic bed	
Estuarine emergent/shrub wetland	Estuarine emergent/shrub wetland	
Unconsolidated shore	Unconsolidated shore	
Barren land	Barren land	
Open water	Open water	
Estuarine forested wetland	Estuarine forested wetland	

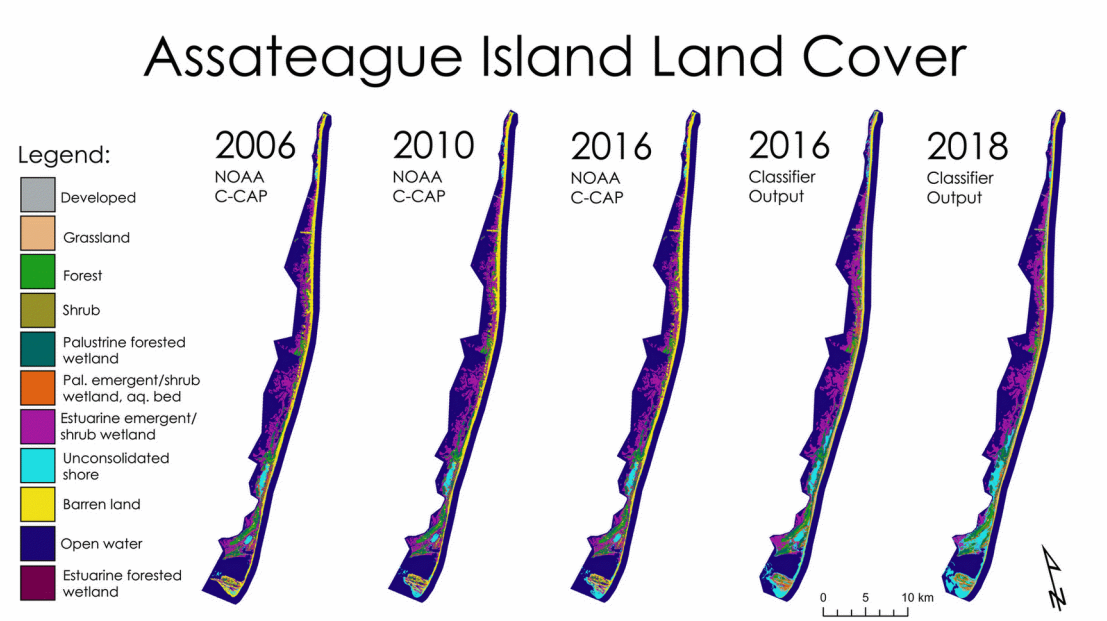

Figure B1. Existing NOAA C-CAP land cover classifications as compared to our Random Forest classifications.

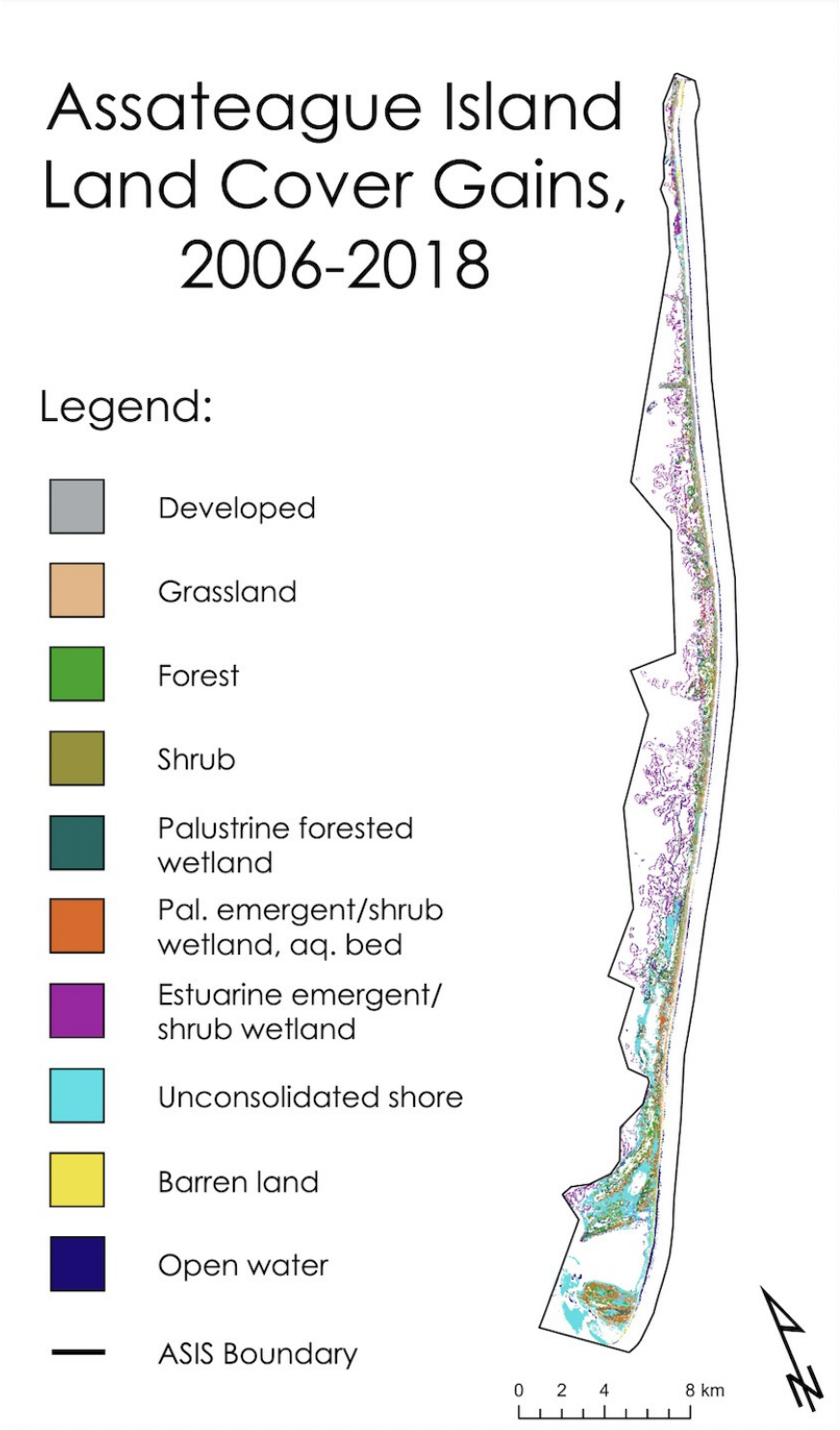

Figure B2. Land cover gains by class from 2006 to 2018.

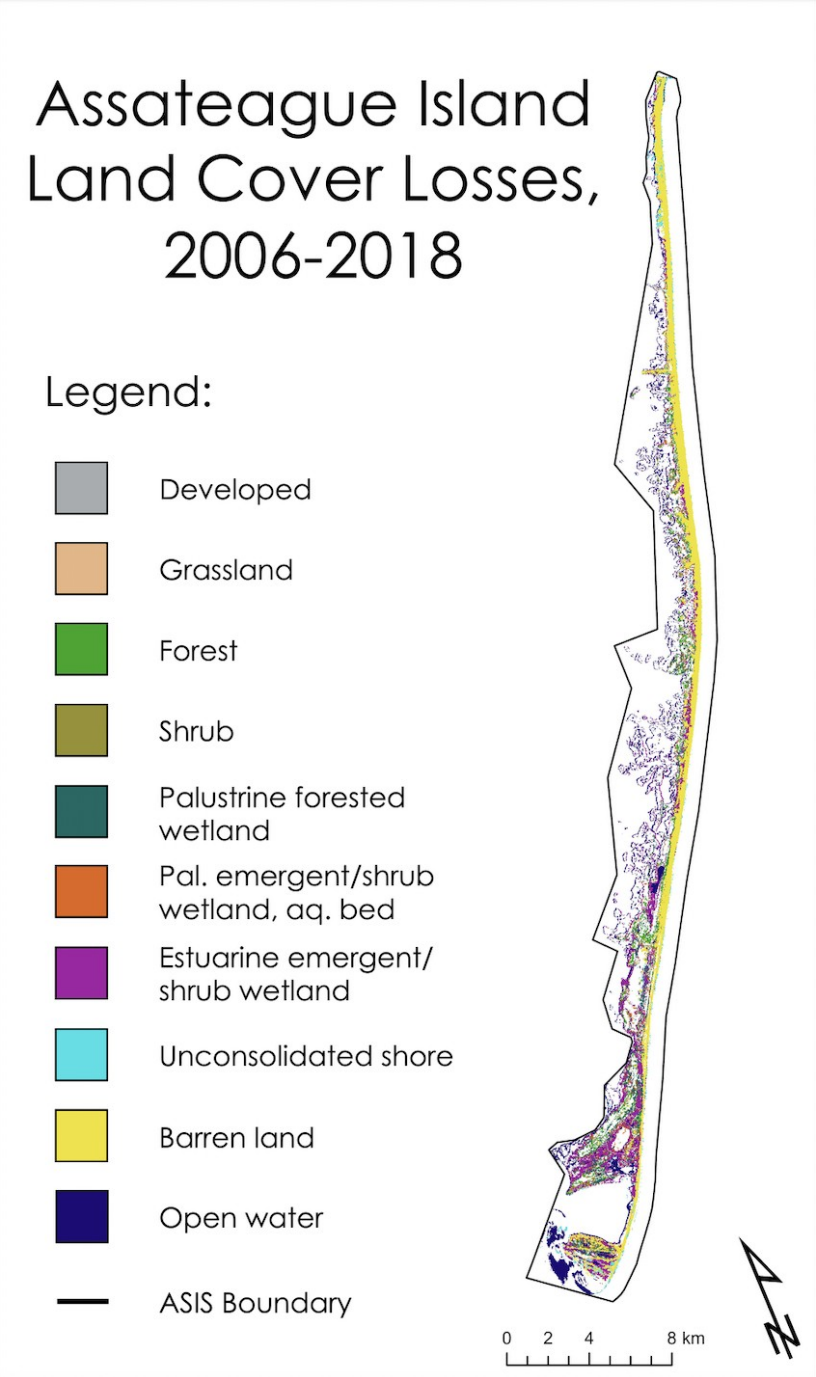

Figure B3. Land cover losses by class from 2006 to 2018.

Appendix C: Landcover Forecasting

Table C1. Calculated loss and gains projected by the 2021 forecast using 2006-2018 historical input data.

Land Cover Type	Predicted Gains [km²]	Predicted Loss [km²]
Developed	1.9	-
Grassland	0.2	-
Forest	0.1	-
Shrub	0.1	-
Palustrine forested wetland	0.06	-
Palustrine emergent shrub/wetland, aquatic bed	0.01	-
Estuarine emergent shrub/wetland	-	0.4
Unconsolidated shore	1.6	-
Barren land	-	2.1
Open water	-	1.6

Table C2. Calculated loss and gains projected by the 2031 forecast using 2006-2018 historical input data.

Land Cover Type	Predicted Gains [km²]	Predicted Loss [km²]
Developed	3.1	-
Grassland	0.2	-
Forest	0.5	-
Shrub	0.3	-
Palustrine forested wetland	0.5	-
Palustrine emergent shrub/wetland, aquatic bed	0.5	-
Estuarine emergent shrub/wetland	-	0.7
Unconsolidated shore	6.3	-
Barren land	-	4.3
Open water	-	6.5

Table C3. Calculated loss and gains projected by the 2046 forecast using 2006-2018 historical input data.

Land Cover Type	Predicted Gains [km²]	Predicted Loss [km²]
Developed	3.2	-

Grassland	-	0.3
Forest	1.2	-
Shrub	0.5	-
Palustrine forested wetland	1.6	-
Palustrine emergent shrub/wetland, aquatic bed	1.0	-
Estuarine emergent shrub/wetland	-	0.6
Unconsolidated shore	11	-
Barren land	-	5.2
Open water	-	13